Colloids and Surfaces B: Biointerfaces 179 (2019) 37–47

Contents lists available at ScienceDirect

Colloids and Surfaces B: Biointerfaces

journal homepage: www.elsevier.com/locate/colsurfb

Tuning surface functionalization and collagen gel thickness to regulate cancer cell migration

Shalini R. Unnikandam Veettil[a], Shawn M. Van Bruggen[a], Doh-Gyu Hwang[c], Michael D. Bartlett[c], Ian C. Schneider[a,b,*]

[a] Department of Chemical and Biological Engineering, Iowa State University, United States
[b] Department of Genetics, Development and Cell Biology, Iowa State University, United States
[c] Department of Materials Science and Engineering, Soft Materials & Structures Lab, Iowa State University, United States

ARTICLE INFO

Keywords:
Interface
Collagen
Adhesion
Morphology
MDA-MB-231
Migration
Durotaxis
Mechanotaxis
Haptotaxis

ABSTRACT

Cancer cells have a tremendous ability to sense and respond to extracellular matrix (ECM) stiffness, modulating invasion. The magnitude of the sensed stiffness can either promote or inhibit the migration of cancer cells out of the primary tumor into surrounding tissue. Work has been done on examining the role of stiffness in tuning cancer cell migration by controlling elastic modulus in the bulk. However, a powerful and complementary approach for controlling stiffness is to leverage interactions between stiff-soft (e.g. glass-hydrogel) interfaces. Unfortunately, most work in this area probes cells in 2D environments. Of the reports that probe 3D environments, none have assessed the role of mechanical linkage to the interface as a potential handle in controlling local stiffness and cell behavior. In this paper, we examine the migration of cancer cells embedded in a collagen fiber network between two flat plates. We examine the role of both surface attachment of the collagen network to the stiff interface as well as thickness (50–540 μm) of the collagen gel in driving collagen organization, cell morphology and cell migration. We find that surface attachment and thickness do not operate overlapping mechanisms, because they elicit different cell responses. While thickness and surface chemistry appear to control morphology, only thickness regulates collagen organization and cell migration speed. This suggests that surface attachment and thickness of the collagen gel control cell behavior through both collagen structure and local stiffness in confined fiber-forming networks.

1. Introduction

Metastasis is the major cause of death due to cancer [1,2]. Invasion into the local extracellular matrix (ECM) is the first step of metastasis and is driven by cell migration. The ECM influences fundamental aspects of cell migration by providing a scaffold on which to migrate and presenting promigratory ligands that the cell can recognize through receptors. Both biophysical and biochemical interactions between cells and the ECM influence cell adhesion, morphology and migration, and thereby play a key role in metastasis [3–6]. Collagen is arguably one of the most important components of the ECM in the tumor microenvironment (TME). Collagen is a fiber forming protein that assembles into an entangled network that can be differentially crosslinked. The density and crosslinking of the collagen network determine the mechanical properties of the network, which are known to change as the tumor progresses [7]. The stiffness in and around tumors increases as the tumor progresses, brought on by enhanced collagen deposition and crosslinking. Cells sense the stiffness of their surroundings by anchoring onto the ECM and exerting traction forces using focal adhesions [8] and can migrate in response to stiffness gradients, resulting in durotaxis [9]. Engineered platforms that can control the mechanical properties of collagen are tremendously useful in understanding how biophysical properties regulate cell migration and other processes germane to cancer metastasis.

Significant research has focused on the characterization of ECM stiffness and its influence on cell behavior, particularly cell migration [10–13]. Most of the studies examining the role of stiffness on cell behavior outline techniques to control the bulk elastic modulus of the ECM by tuning the polymerization parameters such as temperature, concentration, and polymerization time. Furthermore, many studies have examined cell migration in 2D. Several studies have reported an increase in cell speed with increasing ECM elastic modulus. For

* Corresponding author. Present address: Iowa State University, Department of Chemical and Biological Engineering, 2114 Sweeney Hall, Ames, IA, 50011-2230, United States.
E-mail address: ians@iastate.edu (I.C. Schneider).

https://doi.org/10.1016/j.colsurfb.2019.03.031
Received 24 September 2018; Received in revised form 11 March 2019; Accepted 13 March 2019
Available online 16 March 2019
0927-7765/

example, vascular smooth muscle cells [14] and MCF10A epithelial cells [15] have been shown to follow this trend. However, contrasting results have been shown in 3T3 fibroblasts [11]. Thus, it has been theorized that cell migration speed has a biphasic dependence on the stiffness of the ECM [16] with a maximal speed at an optimum elastic modulus, which varies for different cell lines. Furthermore, it was found that cells preferentially move from less stiff region to a stiffer environment, a phenomenon known as durotaxis or mechanotaxis [9,11,12,14,17]. While this has been hypothesized to be important in tumor invasion and metastasis, only recently has it been shown that cancer cells can durotax [9]. Although 2D experimental studies are often easier to conduct and are helpful in broadly uncovering the fundamental aspects of cell behavior by simplifying the intricacies arising from dimensionality, it has been established that 2D and 3D cell responses are characteristically distinct [18,19].

Cells embedded in a 3D system are exposed to a more complex environment with a variety of signals, compared to a 2D monolayer [19]. During 3D migration, the traction forces are transmitted to the matrix through focal adhesions, allowing the cell to remodel the surrounding ECM. Common 3D in vivo mimicking systems are composed of collagen, matrigel, hyaluronan, alginate, gelatin and poly(ethyleneglycol) to name a few [20–25]. In line with the 2D studies, the dependence of cell speed on elastic modulus depends on the cell type [26,27]. In addition, durotaxis can be elicited in 3D environments [28]. Collagen networks represent important environments in which to study the effects of mechanical properties on cell migration due to collagen's abundance and ability to drive cancer cell invasion. However, altering collagen mechanical properties can be challenging. For instance, collagen networks are stiffer at higher densities, but the ligand density increases along with the elastic modulus. Collagen can also be crosslinked using glutaraldehyde or transglutaminase or glycated, stiffening the collagen gel. However, glutaradehyde crosslinking is not compatible with already embedded cells, transglutaminase crosslinking is difficult to control and glycation leads to the formation of advanced glycation end products, thereby changing the chemical composition of the matrix [29]. Other approaches are needed to tune the stiffness of collagen networks. One very powerful completmentary approach is to control stiffness using stiff-soft interfaces. Unfortunately, many of these studies have focused on 2D cell behaviors. Only a handful of papers have assessed the role of stiff-soft interfaces in altering spread area and random migration [27], directed migration [30], focal adhesion formation [31] and myosin activity [28] in 3D. None of this work has examined the role of mechanical linkage of the soft material to the stiff material by tuning the surface chemistry. It is not known if mechanical linkage and proximity to the interface modulate cell behavior similarly or differently. This understanding will help design the surface chemistry to either enhance or diminish the role of the stiff-soft interface in locally controlling stiffness and cell behavior.

In this study we alter the surface chemistry of glass surfaces as well as collagen gel thicknesses to create different biophysical conditions in 3D collagen matrices. By controlling surface chemistry, we altered the strength of adhesion between the functionalized glass and collagen, presumably changing the local stiffness experienced by cells in the matrix close to the surface. The effect of gel thickness on stiffness is governed by the fiber structure of the gel and in fibrous collagen gels, the cell-mediated forces can travel up to a few hundred microns from the surface. We controlled the thickness of the collagen gel from 50 μm to 500 μm in addition to controlling the surface chemistry. Thicker collagen gels had a lower fiber density than thinner collagen gels, but surface chemistry did not seem to have an affect on collagen fiber structure. Cell morphology and migration characteristics were determined under conditions with different surface chemistry and thickness to understand the biophysical effects of matrix parameters arising from polymerization of collagen in 3D chambers. Varying the collagen gel thickness parameters as well as the interfacial adhesion allows us to probe how confinement and stiff-soft interfaces present in the tumor microenvironment influences cell migration.

2. Material and methods

2.1. Surface modifications generating high and low collagen binding surfaces

Glass coverslips (Corning) were cleaned using the squeaky clean procedure described elsewhere [32]. To prepare glutaraldehyde-treated surfaces, the squeaky cleaned coverslips were immersed in a piranha solution, 3:1 H_2SO_4 (Fisher): 30 wt% H_2O_2 (Fisher) v/v, for one hr at room temperature. Next, the coverslips were rinsed three times with nano-pure water and then immersed in a 1% (v/v) 3-aminopropyltriethoxysilane (APTES) (Acros Organics) in a 1 mM aqueous acetic acid (Fisher) solution for 2 h. After the silane coupling reaction, the coverslips were rinsed three times with nano-pure water baked at 100 °C. To treat the coverslips with glutaraldehyde (Electron Microscopy Scinces), they were immersed in a 6% glutaraldehyde solution (v/v) in 1x phosphate buffered saline (PBS) (Gibco) for one hr. Non-binding surfaces were created by treating the squeaky clean glass coverslips with 250 μg ml^{-1} poly(L-lysine)-poly(ethylene glycol) (PLL-PEG) (Alamanda Polymers) in PBS. Coverslips were immersed in PLL-PEG solution and placed on a shaker for five mins and then placed in an incubator (37 °C) overnight (> 12 h).

2.2. Characterization of amine density on glass surfaces

The condensation reaction between primary amines and 4-nitrobenzaldehyde (Sigma Aldrich) in anhydrous ethanol was used as a method to quantify the attachment of APTES to the glass coverslips [33]. The glass coverslips were immersed into a solution containing 0.4 mg ml^{-1} 4-nitrobenzaldhyde and 20 μl acetic acid in 25 ml of anhydrous ethanol at 50 °C for three hrs. After the reaction, the glass coverslips were washed with absolute ethanol and air dried. After drying, the glass coverslips were crushed and immersed in 0.2% aqueous acetic acid solution for one hr at 30 °C, thus liberating the 4-nitrobenzaldehyde from the surface. The absorbance of the solution phase 4-nitrobenzaldehyde was measured using a Cary 50 Bio UV/visible Spectrophotometer (Agilent). Concentrations of APTES on the surface were calculated using a calibration curve prepared from different concentrations of 4-nitrobenzaldehyde in 0.2% acetic acid.

2.3. Contact angle measurement

To test for the successful completion of a glass surface treatment, water contact angles were measured on each surface using a video camera (Javelin) and μManager 1.4 software [34]. A droplet of nanopure water was placed on the surface and imaged through an objective lens (10x, NA = 0.2, Thor Labs, Newton, NJ, USA) attached to the video camera. The collected images were analyzed using the contact angle plugin ImageJ (National Institutes of Health) [35].

2.4. Adhesion characterization

The pull-off force of a glass indenter from an elastic gel as a function of displacement was measured employing the custom-built adhesion apparatus as shown in Fig. 2**a**. The adhesion instrument consists of a functionalized hemi-spherical glass indenter with a diameter of 5 mm, a heating stage and an optical microscope. The glass indenter was glued (cyanoacrylate adhesive) to a small piece of a glass slide that is glued to the head of a screw. Then the screw was inserted into a uniaxial load cell (FUTEK Advanced Sensor Technology, LSB200), which was connected to a piezo-controlled linear actuator (Physik Instruments (PI), N-565). Collagen at 2 mg ml^{-1} concentration in imaging media, was placed within a circular polydimethylsiloxane (PDMS)(Dow Corning Corporation) ring mounted on 25 × 75 x 1 mm glass microscope slide to

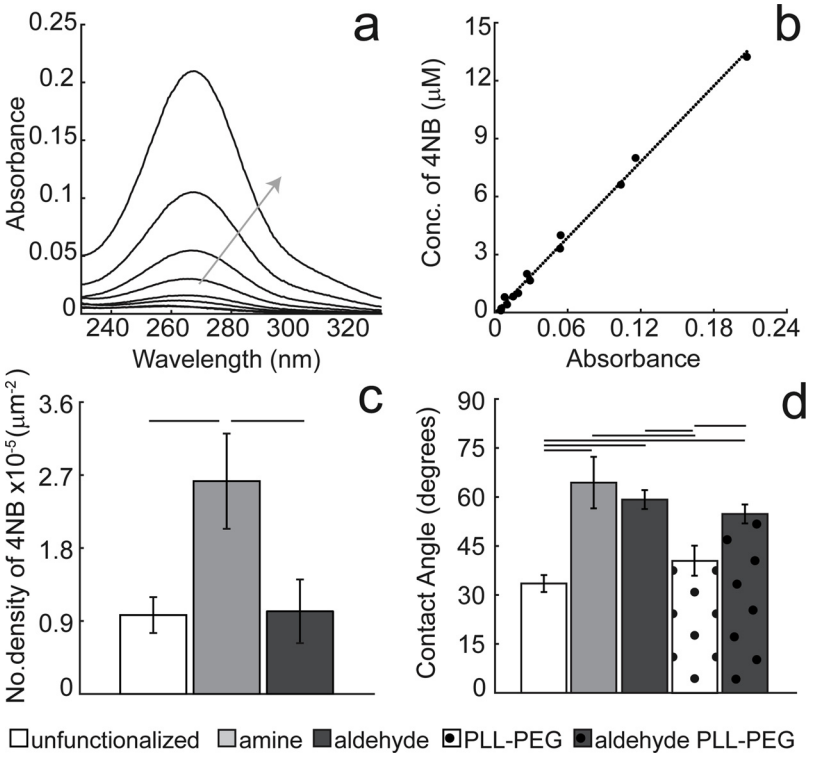

Fig. 1. Characterization of surface properties on functionalized glass surfaces. a) UV absorbance spectra for 4-nitrobenzaldehyde (4NB) at different concentrations (0.10, 0.21, 0.41, 0.83, 1.7, 3.3, 6.6, 13 μM) for one experiment. The gray arrow indicates increasing 4-NB concentrations. b) Standard curve obtained from the absorbance at 270 nm ($N_{experiments} = 2$). c) The number of density 4NB on unfunctionalized, amine functionalized and aldehyde treated glass ($N_{samples} \geq 4$). d) Contact area between water and glass surfaces with different surface functionalization ($N_{samples} \geq 5$). The error bars represent the 95% confidence intervals. Lines over bars indicate that conditions were statistically significantly different as determined by a student's *t*-test with $p = 0.05$.

prevent the specimen from spreading during polymerization. In addition, a dome-shaped glass case with a small circular hole was placed above the glass slide to reduce evaporation. The heating stage (Warner Instruments) on which the glass side was mounted has a circular hole at the center, which enables optical observation of the interface between the indenter and gel throughout the experiments.

Adhesion experiments were performed by bringing the indenter into contact with collagen. The probe was held in contact with the substrate for 30 min. at room temperature, followed by an additional 30 min. at elevated temperature of 37 °C, thereby polymerizing the collagen in situ and crosslinking collagen with the chemically treated surface of the indenter. After the polymerization, the indenter was retracted at a constant displacement rate of 10 μm s^{-1} until complete separation between the probe and collagen gel occurred. The load data were collected with a DAQ (National Instruments, NI USB-6002) in LabVIEW (National Instruments).

2.5. Collagen structural characterization using confocal reflectance microscopy

Collagen at 2 mg ml^{-1} in imaging media was sandwiched between two glass coverslips to form chambers of 50 and 300 μm. The glass coverslips were unfunctionalized or aldehyde treated surfaces. The collagen gel was polymerized for 30 min. at room temperature, followed by an additional 30 min. at elevated temperature of 37 °C. After polymerization, imaging media was added around the gels within the chambers. Images were taken every 4 μm with a Leica SP5 X MP confocal microscope using a 40x (NA = 1.25) oil immersion objective. White light laser set at an excitation wavelength of 488 nm was used for imaging. Backscattered light from a 50/50 pass mirror was collected from the sample. The images were analyzed using ImageJ. The area occupied by and the intensity of the collagen fibers were quatified using a thresholding technique with the grayscale set at a gray value of 20 across all samples.

2.6. Preparation of collagen gel in 3D chambers

MDA-MB-231 cells (human mammary basal/claudin low carcinoma cells, ATCC) were embedded (750,000–1,000,000 cell ml^{-1}) between two glass coverslips to form a chamber in a 2 mg ml^{-1} rat collagen type I solution (Corning) prepared by mixing the imaging media and collagen, keeping the volume to thickness ratio at about 1:20 (μl: μm). Both the bottom and top coverslip were modified with a specific glass surface treatment (glutaraldehyde, squeaky clean glass, or PLL-PEG). The thickness of the chamber was controlled by placing spacers between the two glass coverslips. Additionally, a chamber with a step change in height was created by placing a glass strip on a double-sided tape in a chamber of 300 μm (see Fig. 7a). The solution of collagen and cells was mixed well before being sandwiched between the glasses. The samples were then flipped once every minute for thirty minutes at room temperature to keep the cells evenly distributed within the chamber as the collagen polymerized. The samples were placed in an incubator (37 °C, 5% CO_2) for 30 min to allow the collagen to polymerize further. Finally, imaging media was added to each sample and placed back in the incubator for 24 h. Live cell images were taken in the middle of the chamber on a heating stage at 37 °C and imaged for 8 h at an interval of 2 min. The transmitted images were taken with a 10x (NA = 0.3) objective lens. At least three samples over at least two different days compiled a complete data set.

2.7. Statistical analysis

Analyses of variance (ANOVA) and student *t*-tests were carried out using MATLAB to investigate comparisons when the data sets were normally distributed. The Mann–Whitney U test was run in RStudio, when the normality of the data sets could not be assumed. For all the comparisons, the significance level (α) was set at 0.05 unless otherwise specified. Connecting lines over the conditions indicate the statistical differences in the distributions calculated using the methods mentioned above.

3. Results

3.1. Surface modification of glass generating high and low collagen binding surfaces

High binding surfaces that reacted with collagen were generated through functionalization with APTES and subsequent reaction with a bifunctional aldehyde (glutaraldehyde). We were confident that this functionalization worked because cells spread differently on the different substrates (Supplemental Fig. 1). Amine density after APTES functionalization was measured by UV absorbtion of 4-nitrobenzaldehyde (4-NB) as described in materials and methods (Fig. 1a & b) [33]. The number density was calculated from the amount of 4-NB and the known area of the glass surface. A higher density of 4-NB molecules was recovered from the APTES-treated slides than the unfunctionalized and aldehyde treated surfaces (Fig. 1c). Treating APTES functionalized coverslips with glutaraldehyde abolished the free amines on the surface available for the condensation reaction and brought the number density to background level. The topographical area, which represents the average projected area of APTES over all free orientations is 53.7 $Å^2$ [36]. Since APTES is attached to the surface and likely oriented perpendicular to the surface, we estimated the constrained area covered by a molecule to be approximately 7.2 $Å^2$. Thus, the average fractional surface area covered by APTES molecule is on the order of $0.01 - 0.1$. This indicates that there is low amine surface coverage. To further characterize the surfaces, contact angle measurements were taken. The aldehyde surfaces along with the amine surfaces had much larger contact angles (Fig. 1d) compared to the other surface chemistries, indicating a more hydrophobic surface. All the surface treatments increased the contact angle when compared to the unfunctionalized glass coverslips and this increase indicates surface modification.

3.2. Adhesion of collagen to functionalized glass surfaces

Given changes in surface properties and cell adhesion that were dependent on surface treatment, we measured the adhesion interactions between a collagen gel and functionalized glass hemispheres with three different surface treatments: unfunctionalized, PLL-PEG functionalized, aldehyde functionalized. In these experiments the indenter and collagen gel were brought into contact for a predefined time and temperature and cured in-situ. The indenter was then retracted until complete separation occurs (see Fig. 2a for setup and Section 2.4 for details). We defined two parameters, the maximum adhesive force (F_{max}) which is the maximum tensile load during separation [37,38], and the work of separation, which is the area under the force – displacement curve from the starting point of retraction until the complete separation from the intender and gel (a representative plot is provided in Fig. 2b). F_{max} was measured for three different surface treatments (Fig. 2c). The PLL-PEG functionalization showed the smallest adhesion force between the indenter and the collagen whereas the aldehyde functionalization was the highest. The work of separation for different indenters are shown in Fig. 2d. The observed trends are similar to Fig. 2c, such that the aldehyde-coated indenter showed the highest work of separation. The F_{max} value of the aldehyde functionalized intender was roughly 25% higher than the PLL-PEG and the unfunctionalized glass chemistries. However, the work of separation for the aldehyde condition was only 15% higher than the unfunctionalized intender. We hypothesize that even though the aldehyde-coated indenter creates covalent bonding at the coating-gel interface and is expected to show an increase in pull-off adhesion, because the low amine coverage on the indenter, a less pronounced enhancement of adhesion is seen.

3.3. Quantifying collagen structural organization in chambers with different glass functionalization

Given differences in adhesion of the collagen to the glass under different conditions, we wanted to examine whether the surface chemistry as well as the chamber thickness influenced the structural organization of 3D collagen gels. Qualitatively examining images taken within 5 μm of the surface revealed that thin collagen gels contained fibers that were more densely packed, whereas very little difference was seen across chemistries (Fig. 3**a–d**). The percentage of area occupied by collagen fibers was calculated as a function of distance from the coverslip closest to the objective. This area percentage was higher near the surface for all the conditions (Fig. 3**e** & **f**). Furthermore, it was higher for the 50 μm chambers compared to the 300 μm chambers for both the surface treatments. For the 50 μm chambers, the percentage of area was observed to be a maximum near the glass surfaces and a minimum in the middle of the chamber. A similar trend was observed up to 75 μm into the large 300 μm chambers. However, the collagen fiber organization did not change with the surface treatment. We also quantified fiber intensity (**Fig. S2**). The 300 μm gels were similar in intensities, whereas the 50 μm gel between unfunctionalized coverslips was higher than that for the aldehyde functionalized coverslips. The surface was difficult to find precisely, consequently different stacks form the same conditions were shifted by less than 4 μm and plotted on the same graph. Furthermore, the raw data was fit to a model that incorporated an exponential decrease ($e^{-\alpha z}$) in either the fiber area or intensity due to scattering as you move into the sample and adjusted. This amounted to only small adjustments as the value for α was 0.02 to 0.002 μm^{-1} and depended on density.

3.4. Quantitative cell morphology in 3D collagen chambers with different glass functionalization

After MDA-MB-231 cells were embedded in a 3D collagen chambers (Fig. 4a), cells were fixed and stained for F-actin. The 3D collagen chambers had a thickness of 100 μm or 240 μm, and the glass coverslips were either unfunctionalized or aldehyde functionalized. Fluorescence images were taken and analyzed for cell body area, protrusion length and F-actin intensity at various positions within the chamber. The cell body area was significantly higher in chambers with aldehyde functionalized glass coverslips (Fig. 4b). It was found that the area of the cell does not depend on the thickness of the chamber regardless of the surface chemistry. However, this was an average measure and cells can be various distances from the surface, so the area was calculated as a function of distance from the surface (Fig. 4c).The area of cells embedded in chambers with aldehyde-treated glass coverslips was higher near the surface of the chamber and decreases as the distance from the surface increases. On the other hand, MDA-MB-231 cells in unfunctionalized chambers had a significantly lower area near the glass surface that remained relatively constant as the distance from the surface increases. This result indicated that the cells can sense the attachment of the aldehyde functionalized glass with collagen fibers in the chamber, but only near the stiff-soft interface. Once the cell is far away from the surface, the effect is not observed. Cell protrusion length was also analyzed (Fig. 4d). Cell protrusions in 240 μm chambers were longer than those in 100 μm chambers, but protrusion length was less sensitive to the chemical modification of the coverslips. This was different than cell spreading area, which was primarily dependent on surface chemistry. Finally, measurements of F-actin intensity in the cell body were taken under all four chamber conditions (Fig. 4e). The intensity of cells embedded in the 100 μm chambers was higher than the intensity of cells in the 240 μm chambers, forming an opposite trend to that of the cell protrusion length.

In addition to quantitative metrics of cell morphology, MDA-MB-231 cells embedded in the collagen chambers were also analyzed for their shape. Common cell morphologies were observed within the

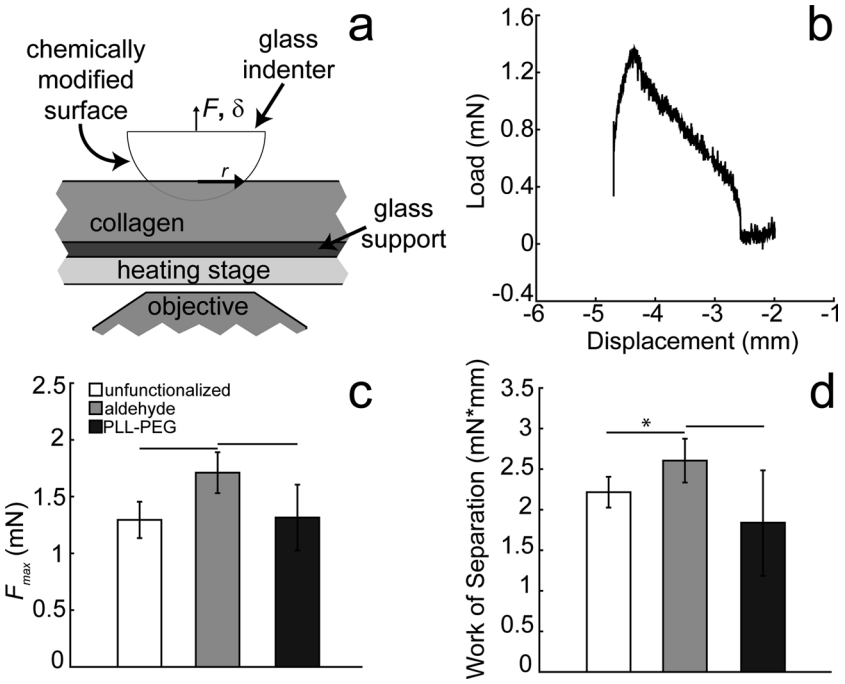

Fig. 2. Characterization of adhesion of collagen to functionalized glass surfaces a) Custom-built adhesion apparatus used to measure the pull-off force of the glass indenter as a function of displacement. b) A representative image of the force-displacement curve obtained from the experiment. c) The corrected pull-off force and d) the work of separation observed when the functionalized glass indenter was in contact with polymerizing collagen. The in situ polymerization of collagen and simultaneous cross-linking of chemically treated glass surfaces with the collagen were carried out with heating stage ($N_{samples} \geq 3$). The error bars represent the 95% confidence intervals. Lines over bars indicate that conditions were statistically significantly different as determined by a student's *t*-test with p = 0.05 and * indicates p = 0.1.

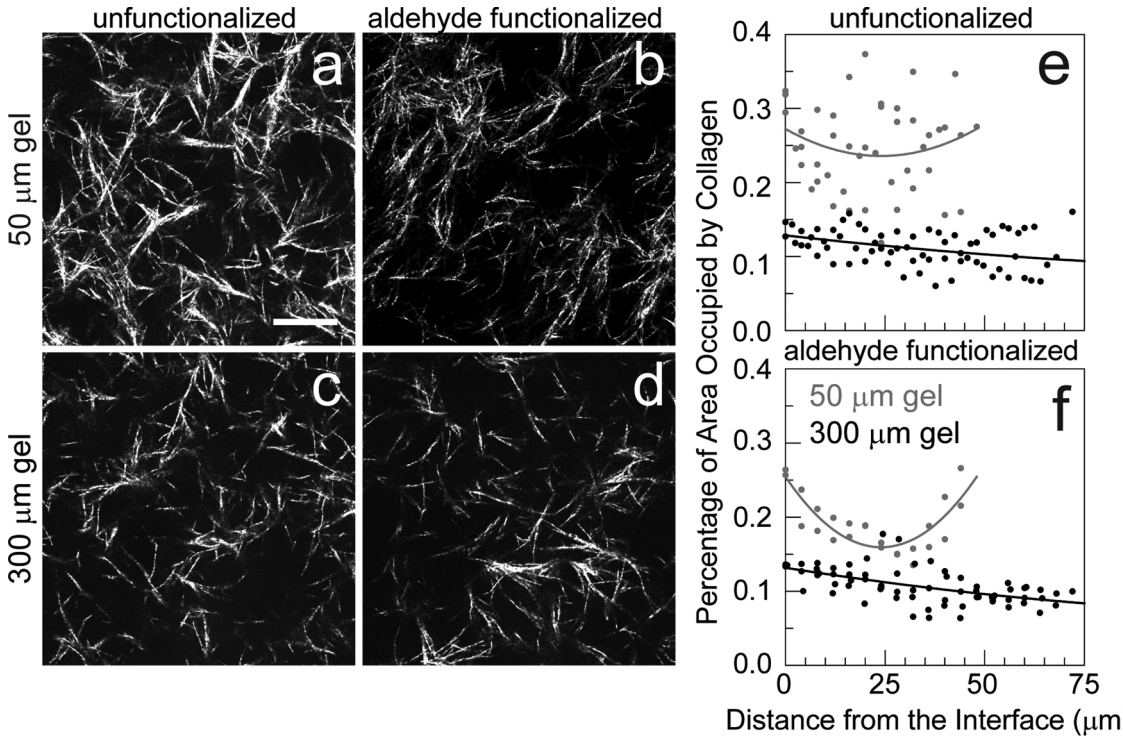

Fig. 3. Characterization of collagen gel structure a), b), c) and d) Collagen gel fibers observed in 3D chambers of 50 μm and 300 μm thicknesses with unfunctionalized and aldehyde treated glass coverslips. The representative images shown are within 5 μm from the interface. e) and f) The percentage of area occupied by collagen observed at intervals of 4 μm from the glass surface (N_{stacks} = 2–4). For the 50 μm chambers, this was quatified for all the planes between the glass surfaces, whereas for the 300 μm chambers, it was calculated for upto 75 μm from one end of the chamber. The lines are a quadratic fit to the data with symmetry about 50 or 300 μm. Scale bar is 20 μm.

chambers and were placed into three general categories (Fig. 5**a–c**). A cell with a round body, no protrusions, and no net polarity in any direction was one cell morphology identified in the chambers (Fig. 5a). Alternatively, a cell with a polarity as it has a single protrusion on one side of the cell was also observed (Fig. 5b). The third type of cell morphology found in the chamber was a cell with an elongated body and two primary protrusions on both ends of the cell body (Fig. 5c). The fraction of cells displaying the three morphologies in the various collagen chamber conditions was analyzed (Fig. 5**d–f**). The thickness of the chamber regulated the presence of polar (Fig. 5b) and non-polar cells (Fig. 5**a** & **c**). Collagen chambers of the 240 μm thickness had a larger fraction of cells displaying the polar morphology (Fig. 5**b** & **e**) than the non-polar, rounded morphology (Fig. 5**a** & **c** & **d** & **f**) regardless of the surface chemistry used. In addition, the fraction of cells with an

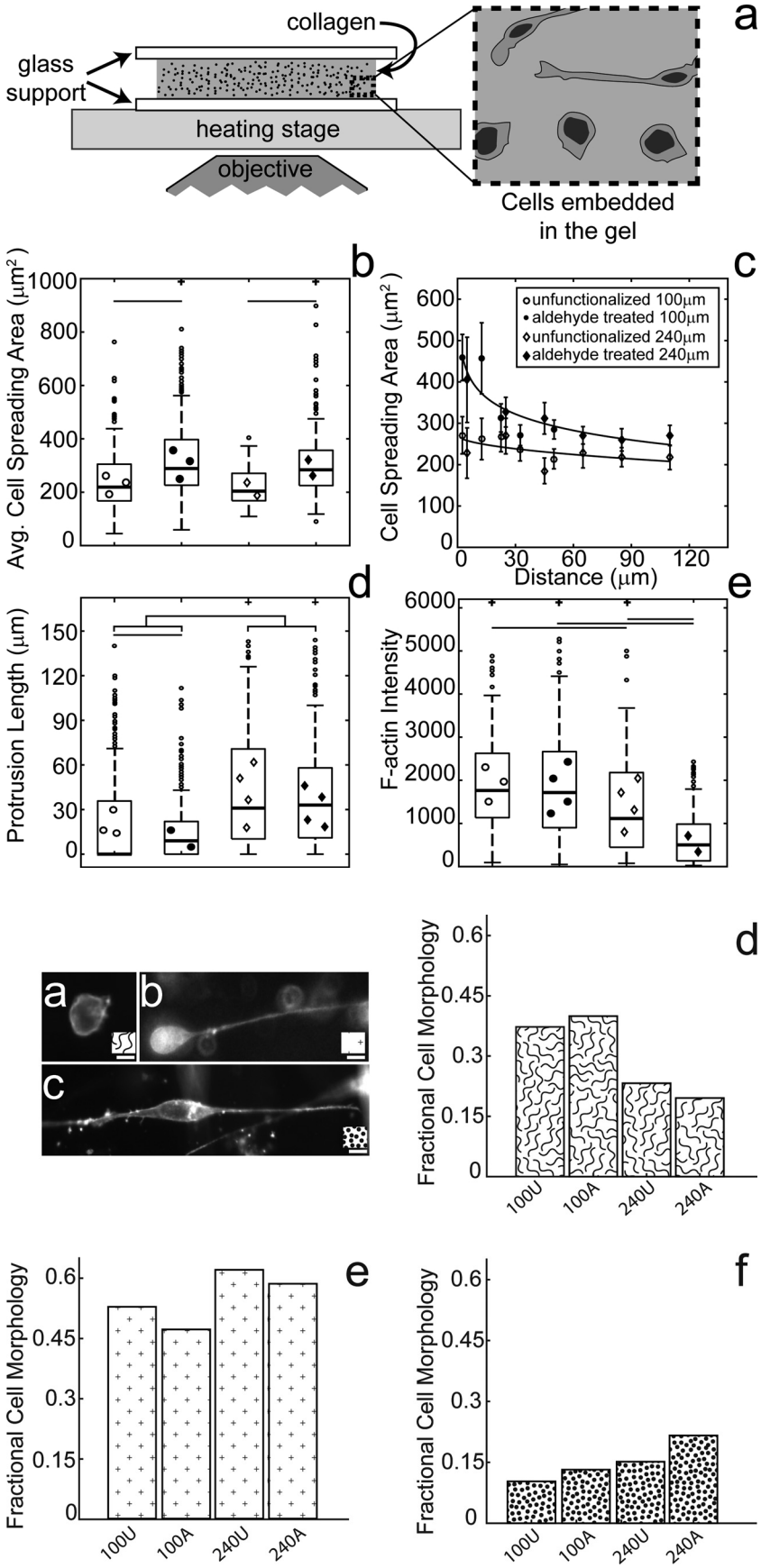

Fig. 4. Characterization of cell morphology in 3D collagen chambers of different thicknesses and glass functionalization a) Schematic representation of imaging set up with cells embedded in collagen gel. b) Cell spreading area, d) protrusion length and e) F-actin intensity averaged over thickness for 100 μm and 240 μm chambers of unfunctionalized and aldehyde functionalized coverslips. c) Cell spreading area observed at intervals of 5 μm and 10 μm for 100 μm and 240 μm collagen chambers with unfunctionalized and aldehyde functionalized glass surfaces, respectively ($N_{samples} = 3$, $N_{cells} \geq 99$ for b,d & e, $N_{samples} = 3$, $N_{cells} \geq 9$ for c). The error bars represent the 95% confidence intervals. In the box plots, the middle line indicates median, the top and bottom of the box indicate 75th percentile and 25th percentile respectively, and the whiskers indicate the 90th and 10th percentiles. Lines over bars indicate that conditions were statistically significantly different as determined by an ANOVA test with $p = 0.05$. + indicates that there are values outside the range of y-axis.

Fig. 5. Characterization of cell shape in 3D collagen chambers of different thicknesses and glass functionalization. Different cell morphologies were found for all surface conditions and chamber thicknesses. The cells were grouped according to the following cell morphologies: a) round and non-polar, b) round and polar, c) skinny and non-polar. Roundness is determined by the cell body while polarity is determined by the protrusions. Fractional cell morphology observed in 100 μm and 240 μm chambers with unfunctionalized and aldehyde treated conditions for d) round and non-polar, e) round and polar and f) skinny and non-polar morphologies ($N_{samples} = 3$, $N_{cells} \geq 99$ for a given thickness and surface chemistry). All scale bars are 10 μm.

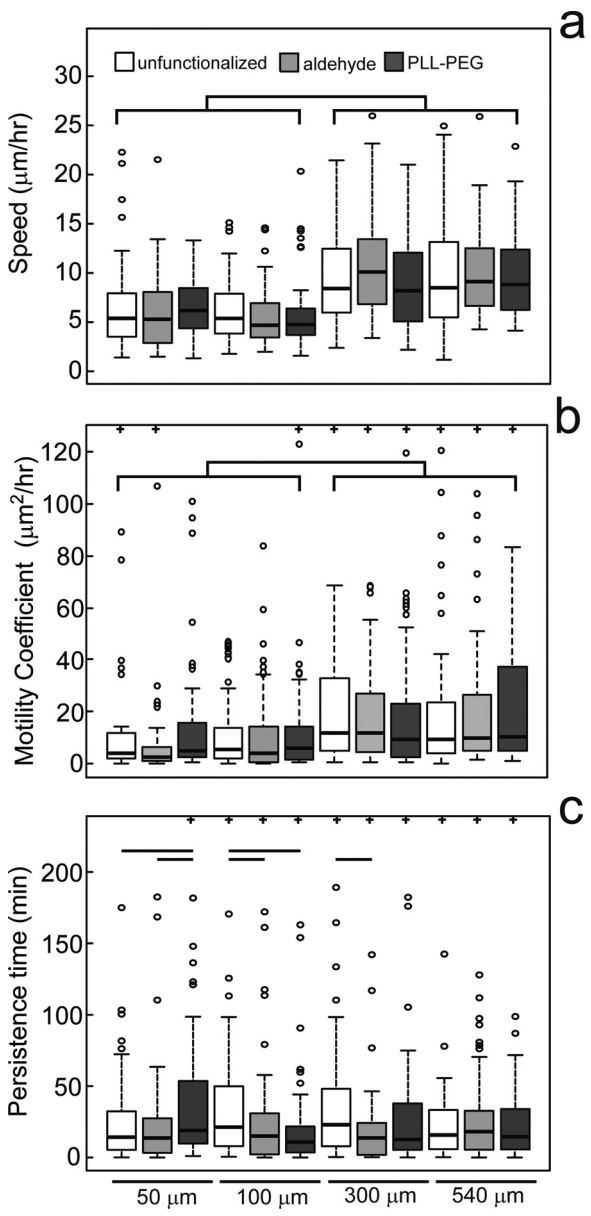

Fig. 6. Motility characterization in 3D collagen chambers with functionalized glass surfaces. Migration analysis of MDA-MB-231 cells embedded in 2 mg ml^{-1} collagen gel chambers with different gel thicknesses and surface chemistries. a) Cell migration speed, b) motility coefficient and c) persistence time of MDA-MD231 cells observed in the middle of the chamber ($N_{samples} \geq 3$, $N_{cells} \geq 44$). The cell migration speed and motility coefficient were found to be larger in the thick chambers (300 μm and 540 μm) than the thin chambers (50 μm and 100 μm). In the box plots, the middle line indicates median, the top and bottom of the box indicate 75th percentile and 25th percentile respectively, and the whiskers indicate the 90th and 10th percentiles. Lines over bars indicate that conditions were statistically significantly different as determined by a Mann-Whitney U test with $p = 0.05$. + indicates that there are values outside the range of y-axis.

elongated, non-polar morphology (Fig. 5**c**&**f**) did not dramatically change under different surface modifications or chamber thicknesses.

3.5. Cell motility in 3D collagen chambers with different glass functionalization

Cell migration was observed in the middle of the chambers for different gel thicknesses. Cell speed and motility coefficient were dependent on the gel thickness, but the data did not provide evidence to suggest that surface treatment affected these motility properties. The cell speed and motility coefficient as both were found higher in the thick chambers (300 μm and 540 μm) in comparison to the thin chambers (50 μm and 100 μm) (Fig. 6**a**&**b**). However, persistence time calculations provided a differential response to cues arising from surface chemistries (Fig. 6c). The persistence time was found to be greater in the PLL-PEG at a chamber height of 50 μm, whereas in the 100 μm chamber it was larger in the unfunctionalized condition when compared with the other conditions. In the 300 μm chamber, the persistence time in the unfunctionalized condition was found to be larger than the aldehyde treated condition (Fig. 6c). Taken together, cell speed and motility coefficient were not dependent on surface functionalization, but were dependent on collagen gel thickness, whereas persistence time tended to be more dependent on surface functionalization, but in a collagen gel thickness manner.

The differential cell response with gel thickness, observed in cell speed and the motility coefficient led us to examine cell behavior in a system with a step change comprising a thick side (300 μm) and a thin side (50 μm) (Fig. 7a). The orientation of cell alignment near the boundary of the step change was measured and directionality index for static, but oriented cells was quantified at 2 and 16 h after embedding cells in the collagen gel. It was observed that the directionality index increased after 16 h for the thick and the thin sides when compared to the cell orientation after 2 h. The cells at the thick side had a higher directionality index than the thin side after 16 h (Fig. 7b). In addition to this, when the cell orientation was examined as a function of distance from the boundary of the step, a higher directionality index was observed for the thick side compared to the thin side after 16 h for both surface chemistries (Fig. 7**c** & **d**). However, this trend was not observed at 2 h, suggesting that it takes time for cells to develop an orientation. Along with orientation, we examined cell migration. The migration studies showed that a higher migration speed was observed in the thick side of the chamber (Fig. 7e). The migration speeds in the thick and the thin sides of the chamber were comparable with the migration speeds observed in the chambers of gel thicknesses of 50 μm and 300 μm, respectively (Figs. 7e vs. 6 **a**). Motility coefficient was also found to be higher in the thick side of the chamber for the unfunctionalized condition (Fig. 7f). However, there was no statistical difference for the aldehyde treated condition. The persistence time of cell migration was also calculated. The data did not suggest that there was a difference between the distributions for the thin and thick sides statistically, however there was a difference between chemistries in the thick side (Fig. 7g). We also examined directional migration. Directional cell migration was observed in the thick side of the chamber. These cells showed a positive, non-zero directionality index for both unfunctionalized and aldehyde treated conditions (Fig. 7h). These results indicated that thickness can alter directional sensing, reorienting cells towards interfaces over time. However, migration in the direction of the interface only occured on the thick side.

4. Discussion

Collagen is an important and abundant protein in the TME and consequently, many studies have focused on methods for altering the mechanical properties within collagen gels including altering the concentration, temperature of polymerization and gelation time [39]. In addition, crosslinking through glutaraldehyde, transglutaminase, lysl oxidase or glycation has been shown to increase the stiffness of collagen gels [40,41]. However, these techniques have drawbacks including changes in collagen gel properties other than stiffness, difficulty in controlling the stiffness and incompatibility with already embedded cells. As an alternative approach, local stiffness can be controlled based on the distance between the cell and the stiff-soft interface, a parameter frequently controlled by the thickness of the soft material. Several studies have examined the regulation of thickness or position with respect to a stiff-soft interface to alter local stiffness, but none have

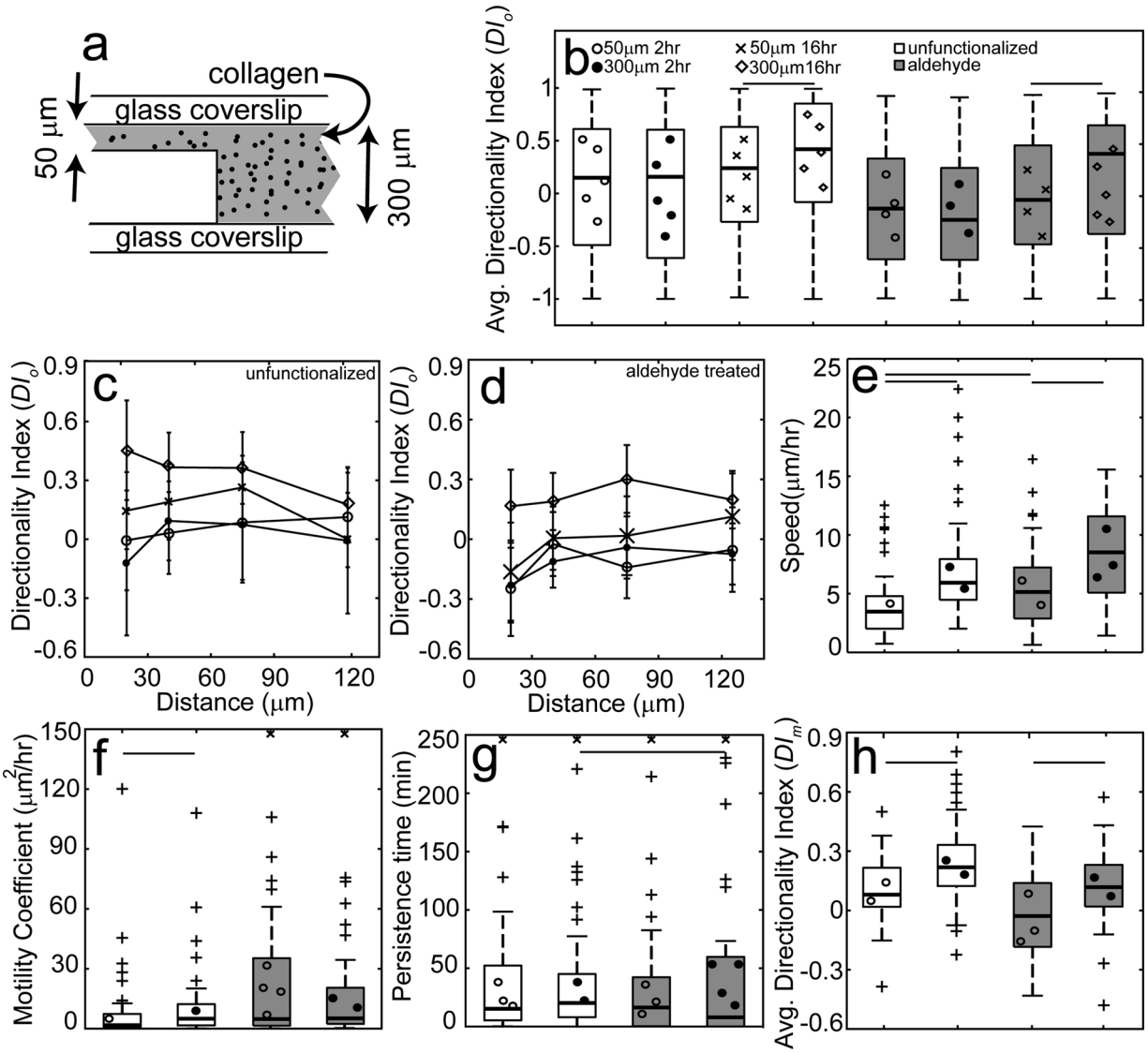

Fig. 7. Motility characterization in 3D collagen chambers with step change in thickness. a) Schematic representation of a step change in the collagen gel. Migration and directionality analysis of MDA-MB-231 cells embedded in 2 mg ml^{-1} collagen gel chambers, observed at the boundary of a step change in the thickness ($N_{samples} \geq 4$, $N_{cells} \geq 75$ for b, $N_{cells} \geq 12$ for c, $N_{cells} \geq 21$ for d, $N_{samples} \geq 4$, $N_{cells} \geq 36$ for e–h). b) Orientation directionality index averaged over distance from the boundary of the step change for 50 and 300 μm gel thicknesses. c) & d) Orientation directionality index as a function of distance from the boundary. e) The cell migration speed, f) motility coefficient, g) persistence time and h) migration directionality index averaged over the cells in the 50 and 300 μm sides of the chambers with unfunctionalized and aldehyde treated surface conditions. The error bars represent the 95% confidence intervals. In the box plots, the middle line indicates median, the top and bottom of the box indicate 75th percentile and 25th percentile respectively, and the whiskers indicate the 90th and 10th percentiles. Lines over bars indicate that conditions were statistically significantly different as determined by ANOVA test with $p = 0.05$ or a Mann-Whitney *U* test with $p = 0.05$. x indicates that there are values outside the range of y-axis.

examined the role of surface attachment in regulating local stiffness and cell behavior. Our primary interest was to assess the role of surface attachment of collagen within the collagen gel to a stiff glass surface. We wanted to know if mechanical linkage of the soft material to the stiff material at the interface altered cell behavior similarly to distance. We assessed the adhesion of the collagen gel to the stiff glass surface under different functionalization methods by polymerizing the collagen gel in the presences of differentially functionalized glass beads. While we did not see dramatic changes in the adhesion force (˜30% increase), this is likely due to the low coverage of the amine and consequently, aldehyde functionalization. Although, the aldehyde functionalized surface showed a larger pull-off force and work of separation as expected, there was no significant difference between the PLL-PEG and unfunctionalized conditions. This approach of controlling attachment of the soft material to a stiff interface complements other approaches that modulate bulk stiffness.

Given that surface functionalization changed the adhesion between the collagen and the glass surface, we perturbed surface functionalization and collagen gel thickness in order to assess their influence on cell morphology and cell migration. Our original hypothesis was that one could tune the local stiffness in the collagen gel through either the surface attachment or position with respect to the stiff-soft interface, the latter being controlled by the thickness of the collagen gel. Stronger attachment and smaller distances from the interface would result in higher local stiffnesses. Cell area and fraction of cells that were extended and polarized were both dependent on surface chemistry and distance from the surface (or gel thickness) in a way that was consistent with the hypothesis that we were controlling local stiffness through either surface attachment or thickness. Surprisingly, other morphological and migration parameters showed no such trend. Protrusion

length, F-actin content and the fraction of polarized cells were not dependent on distance from the stiff-soft interface or surface functionalization, yet they were primarily dependent on the thickness of the collagen gel. In addition, migration speed, motility coefficient and directionality index for durotaxis showed no dependence on surface functionalization, but rather thickness only. Finally, persistence time depended only on surface functionalization and not gel thickness. While surface functionalization and collagen gel thickness jointly regulate local stiffness, other mechanisms could influence cell behavior. For instance, we measured collagen fiber density and showed that thin gels were more dense than thick gels, but surface chemistry played an undetectable role in altering collagen fiber density. This thickness-dependent collagen fiber density has been shown elsewhere, but for gels that were orders of magnitude thicker [42]. The same insensitivity to surface chemistry is found in cell migration speed. The less dense collagen fiber networks resulted in faster migration. Perhaps cell migration is driven by collagen fiber density, whereas cell morphology is driven by stiffnesss. Alternatively, cells secrete diffusible pro-migratory factors into the medium. The local concentrations of these factors depend on the distance to the stiff-soft interface (Supplemental Fig. 3). Since the concentration boundary condition at the stiff-soft interface is a no flux boundary condition, this enhances the concentration due to the reflective nature of the boundary. However, absent of binding of the factors to the interface, surface chemistry should not affect this mechanism. If cell morphology or migration is dependent on secreted diffusible factors, a distance or thicknesss dependence would occur.

To our knowledge no cell studies have examined the role of surface attachment of soft materials to stiff materials. However, several groups have examined the role of gel thickness or distance from the surface. Numerous 2D studies have shown that the thickness of soft gels attached to a stiff surfaces alters cell spreading area, where thick gels result in small spread areas and thin gels result in large spread areas [43–48]. Interestingly, fiber forming matrices like those composed of fibrin or collagen appear to affect cell behavior further away from the surface as compared to gels like polyacrylamide, even when the bulk modulus is similar [49]. Fiber forming gels can exert changes on cell spreading areas up to about 150 μm away from the surface. The distance over which the area decreases by 50% for fiber forming gels appears to be around 80 μm, whereas that for polyacrylamide is about 4 μm [49]. Migration speed does not show such simple behavior. Migration speed increased in mesenchymal cells and decreased in fibroblasts with thicker gels [50]. This is to be expected as migration has a biphasic response to stiffness and depending on the cell type and the elastic modulus of the gel, the stiffer environment could either act to increase or decrease speed. Finally, gel thickness appears to modulate collective cell migration and durotactic movement during the clustering of cells [51]. Fewer studies on the effect of stiffness have been conducted in 3D. Glioblastoma cells embedded in matrigel were shown to decrease their area and aspect ratio as the distance between the interface and the cell increased [27]. Similar to 2D, the penetration depth of the effect appears to be on the order of 150 μm. Furthermore, migration speed was fast, close to the stiff-soft interface and slower further away from the interface. Fibroblasts in collagen also showed the same area dependence as glioblastoma cells in matrigel, however, they did not appear to alter their migration speed [30]. Finally, while surface attachment has not been quantitatively altered, attached vs. floating collagen gels have been compared and fibroblasts appear to decrease their migration speed in collagen gels that are not attached to a stiff interface [52]. This change in migration may possibly be due to the change in focal adhesions, which seem to disappear when more than 200 μm from the surface [53]. The area dependence of MDA-MB-231 cells in collagen on distance seems to be a bit blunted as compared to glioblastoma, fibroblasts or mesenchymal cells. We only observed differences over ~60 μm and only in situations where collagen was covalently attached to the glass. This could be a function of diminished mechanosensing in MDA-MB-231 cells or the presence of additional mechanisms beyond local stiffness modulation described in the previous paragraph. In addition, MDA-MB-231 cells appear to increase their migration speed in thicker collagen gels, but because this affect was not altered as a function of surface attachment of collagen, perhaps migration too depends on mechanisms beyond local stiffness modulation.

This change in stiffness as a function of distance from a stiff-soft interface can also be leveraged to induce durotaxis, directed migration in response to a stiffness gradient. However, only recently has it been shown that cancer cells can durotax [9]. Work in other cell lines has been conducted on 2D substrates, where the surface stiffness has been controlled by underlying topographical features [12,54]. In 3D, durotactic gradients have been formed in constant thickness collagen gels attached to polyacrylamide gels with gradients of stiffness [28] or in gels with step changes in surface features [50]. Within the collagen gels formed over step changes, durotaxis occurred from soft to stiff (thick to thin section) with the relevant changes occurring from 100 to 40 μm thick collagen gels. The directionality found in our cells moving from 300 to 50 μm is somewhat larger, but matches well with those for fibroblasts and mesenchymal stem cells. However, because density appears to differ between thick and thin sections (Fig. 3) haptotaxis, directed migration in response to gradients of ECM, might also play a role both in this study as well as in a previous study [50]. Patterning surface attachment of the soft material to a stiff interface or designing complex topographical structures is an interesting way to guide cell migration through durotaxis or haptoaxis in devices. These approaches afford the ability to fabricate surfaces well before cell embedding in the soft material, thus allowing the engineered features of the surface to imprint spatial gradients of stiffness or fiber density into the 3D gel and eliminating the need to create gradients in bulk properties like elastic modulus. Understanding how mechanical linkage to this structure affects cell behavior is abosulelty critical to the design of these devices.

5. Conclusions

In this paper we examined the role of surface chemistry and collagen gel thickness in controlling collagen structure, cell morphology and migration of MDA-MB-231 breast cancer cells in 3D collagen gels. We find that surface attachment and thickness do not operate overlapping mechanisms, because they elicit different cell responses. Aldehyde functionalized glass in comparison to PLL-PEG or unfunctionalized glass is more adhesive to collagen, presumably increasing the observed stiffness close to the glass-collagen gel interface. Collagen fiber density was highest in thin gels as compared to thick gels, but surface chemistry did not regulate fiber density. Cell spreading area in 3D collagen gels depended on the proximity of the cell to the glass-collagen interface, but only when glass was aldehyde functionalized and glass-collagen adhesion was largest. Unfunctionalized glass showed no area dependence on distance from the glass-collagen interface. Cell migration differed. Cells migrated with higher speeds in thick collagen gels and appeared to show no dependence on the glass surface chemistry. Finally, directional migration could be induced by leveraging step changes in the thickness of the collagen. The work from this paper shows that while surface chemistry and collagen gel thickness can be used to alter the stiffness, they affect cell properties differently, suggesting additional mechanisms that may cooperate with stiffness in driving cell migration in confined ECM.

Competing interests

The authors declare no competing interests.

Contributions

SRUV conducted the experiments in Figs. 1,2,3,6,7, S1 and S2 and conceived the experiments in Fig. 7. SMVB conducted the experiments

in Figs. 1, 4, 5 and S2 and conceived the experiments in Fig. 1. DGH conducted and conceived the experiments in Fig. 2. ICS conceived the experiments in all figures. MDB conceived the experiments in Fig. 2. ICS, SRUV, SMVB, DGH and MBD wrote the manuscript.

Acknowledgements

This work was supported by a seed grant from the College of Engineering at Iowa State University as well as start-up funds from the Department of Materials Science and Engineering. Shawn Van Bruggen was supported by a National Science Foundation Research Experience for Undergraduates grant [1560012]. We acknowledge Margaret Carter and the Roy J. Carver High Resolution Microscopy Facility for help with the confocal reflectance microscopy.

Appendix A. Supplementary data

Supplementary material related to this article can be found, in the online version, at doi:https://doi.org/10.1016/j.colsurfb.2019.03.031.

References

[1] S. Valastyan, R.A. Weinberg, Tumor metastasis: molecular insights and evolving paradigms, Cell 147 (2011) 275–292, https://doi.org/10.1016/j.cell.2011.09.024.
[2] P. Mehlen, A. Puisieux, Metastasis: a question of life or death, Nat. Rev. Cancer 6 (2006) 449–458, https://doi.org/10.1038/nrc1886.
[3] F. Gattazzo, A. Urciuolo, P. Bonaldo, Extracellular matrix: a dynamic microenvironment for stem cell niche, Biochim. Biophys. Acta Gen. Subj. 1840 (2014) 2506–2519, https://doi.org/10.1016/j.bbagen.2014.01.010.
[4] J.K. Mouw, G. Ou, V.M. Weaver, Extracellular matrix assembly: a multiscale deconstruction, Nat. Rev. Mol. Cell Biol. 15 (2014) 771–785, https://doi.org/10.1038/nrm3902.
[5] C. Bonnans, J. Chou, Z. Werb, Remodelling the extracellular matrix in development and disease, Nat. Rev. Mol. Cell Biol. 15 (2014) 786–801, https://doi.org/10.1038/nrm3904.
[6] S.L.K. Bowers, I. Banerjee, T.A. Baudino, The extracellular matrix: at the center of it all, J. Mol. Cell. Cardiol. 48 (2010) 474–482, https://doi.org/10.1016/j.yjmcc.2009.08.024.
[7] K. Polyak, I. Haviv, I.G. Campbell, Co-evolution of tumor cells and their microenvironment, Trends Genet. 25 (2009) 30–38, https://doi.org/10.1016/j.tig.2008.10.012.
[8] U.S. Schwarz, M.L. Gardel, United we stand – integrating the actin cytoskeleton and cell–matrix adhesions in cellular mechanotransduction, J. Cell. Sci. 125 (2012) 3051–3060, https://doi.org/10.1242/jcs.093716.
[9] B.J. DuChez, A.D. Doyle, E.K. Dimitriadis, K.M. Yamada, Durotaxis by human cancer cells, Biophys. J. 116 (2019) 670–683, https://doi.org/10.1016/j.bpj.2019.01.009.
[10] A. Pathak, S. Kumar, Independent regulation of tumor cell migration by matrix stiffness and confinement, Proc. Natl. Acad. Sci. 109 (2012) 10334–10339, https://doi.org/10.1073/pnas.1118073109.
[11] C.M. Lo, H.B. Wang, M. Dembo, Y.L. Wang, Cell movement is guided by the rigidity of the substrate, Biophys. J. 79 (2000) 144–152, https://doi.org/10.1016/S0006-3495(00)76279-5.
[12] D.S. Gray, J. Tien, C.S. Chen, Repositioning of cells by mechanotaxis on surfaces with micropatterned Young's modulus, J. Biomed. Mater. Res. Part A 66 (2003) 605–614, https://doi.org/10.1002/jbm.a.10585.
[13] D.E. Discher, Tissue cells feel and respon to the stiffness of their substrate, Science (80) 310 (2005) 1139–1143, https://doi.org/10.1126/science.1116995.
[14] B.C. Isenberg, P.A. DiMilla, M. Walker, S. Kim, J.Y. Wong, Vascular smooth muscle cell durotaxis depends on substrate stiffness gradient strength, Biophys. J. 97 (2009) 1313–1322, https://doi.org/10.1016/j.bpj.2009.06.021.
[15] M.R. Ng, A. Besser, G. Danuser, J.S. Brugge, Substrate stiffness regulates cadherin-dependent collective migration through myosin-II contractility, J. Cell Biol. 199 (2012) 545–563, https://doi.org/10.1083/jcb.201207148.
[16] B.L. Bangasser, S.S. Rosenfeld, D.J. Odde, Determinants of maximal force transmission in a motor-clutch model of cell traction in a compliant microenvironment, Biophys. J. 105 (2013) 581–592, https://doi.org/10.1016/j.bpj.2013.06.027.
[17] J.Y. Wong, A. Velasco, P. Rajagopalan, Q. Pham, Directed movement of vascular smooth muscle cells on gradient-compliant hydrogels, Langmuir 19 (2003) 1908–1913, https://doi.org/10.1021/la026403p.
[18] A.S. Meyer, S.K. Hughes-Alford, J.E. Kay, A. Castillo, A. Wells, F.B. Gertler, D.A. Lauffenburger, 2D protrusion but not motility predicts growth factor-induced cancer cell migration in 3D collagen, J. Cell Biol. 197 (2012) 721–729, https://doi.org/10.1083/jcb.201201003.
[19] B.M. Baker, C.S. Chen, Deconstructing the third dimension – how 3D culture microenvironments alter cellular cues, J. Cell Sci. 125 (2012) 3015–3024, https://doi.org/10.1242/jcs.079509.
[20] S. Geraldo, A. Simon, N. Elkhatib, D. Louvard, L. Fetler, D.M. Vignjevic, Do cancer cells have distinct adhesions in 3D collagen matrices and in vivo? Eur. J. Cell Biol. 91 (2012) 930–937, https://doi.org/10.1016/j.ejcb.2012.07.005.
[21] S.T. Kreger, S.L. Voytik-Harbin, Hyaluronan concentration within a 3D collagen matrix modulates matrix viscoelasticity, but not fibroblast response, Matrix Biol. 28 (2009) 336–346, https://doi.org/10.1016/j.matbio.2009.05.001.
[22] Z. Li, S. Huang, Y. Liu, B. Yao, T. Hu, H. Shi, J. Xie, X. Fu, Tuning alginate-gelatin bioink properties by varying solvent and their impact on stem cell behavior, Sci. Rep. 8 (2018), https://doi.org/10.1038/s41598-018-26407-3.
[23] M. Cavo, M. Caria, I. Pulsoni, F. Beltrame, M. Fato, S. Scaglione, A new cell-laden 3D Alginate-Matrigel hydrogel resembles human breast cancer cell malignant morphology, spread and invasion capability observed "in vivo", Sci. Rep. 8 (2018) 5333, https://doi.org/10.1038/s41598-018-23250-4.
[24] E. Gontran, M. Juchaux, C. Deroulers, S. Kruglik, N. Huang, M. Badoual, O. Seksek, Assessment of the ability of poly(l-lysine)–poly(ethylene glycol) (PLL–PEG) hydrogels to support the growth of U87-MG and F98 glioma tumor cells, J. Appl. Polym. Sci. 135 (2018) 46287, https://doi.org/10.1002/app.46287.
[25] K.M. Hakkinen, J.S. Harunaga, A.D. Doyle, K.M. Yamada, Direct comparisons of the morphology, migration, cell adhesions, and actin cytoskeleton of fibroblasts in four different three-dimensional extracellular matrices, Tissue Eng. Part A 17 (2011) 713–724, https://doi.org/10.1089/ten.tea.2010.0273.
[26] M.H. Zaman, L.M. Trapani, A.L. Sieminski, D. MacKellar, H.Y. Gong, R.D. Kamm, A. Wells, D.A. Lauffenburger, P. Matsudaira, A. Siemeski, D. MacKellar, H.Y. Gong, R.D. Kamm, A. Wells, D.A. Lauffenburger, P. Matsudaira, Migration of tumor cells in 3D matrices is governed by matrix stiffness along with cell-matrix adhesion and proteolysis, Proc. Natl. Acad. Sci. 103 (2006) 10889–10894, https://doi.org/10.1073/pnas.0604460103.
[27] S.S. Rao, S. Bentil, J. DeJesus, J. Larison, A. Hissong, R. Dupaix, A. Sarkar, J.O. Winter, Inherent interfacial mechanical gradients in 3D hydrogels influence tumor cell behaviors, PLoS One 7 (2012) e35852, , https://doi.org/10.1371/journal.pone.0035852.
[28] M. Raab, J. Swift, P. Dingal, P. Shah, J.W. Shin, D.E. Discher, Crawling from soft to stiff matrix polarizes the cytoskeleton and phosphoregulates myosin-II heavy chain, J. Cell Biol. 199 (2012) 669–683, https://doi.org/10.1083/jcb.201205056.
[29] B.N. Mason, C.A. Reinhart-King, Controlling the mechanical properties of three-dimensional matrices via non-enzymatic collagen glycation, Organogenesis 9 (2013) 70–75, https://doi.org/10.4161/org.24942.
[30] C.H. Feng, Y.C. Cheng, P.H.G. Chao, The influence and interactions of substrate thickness, organization and dimensionality on cell morphology and migration, Acta Biomater. 9 (2013) 5502–5510, https://doi.org/10.1016/j.actbio.2012.11.024.
[31] S.I. Fraley, Y. Feng, R. Krishnamurthy, D.-H. Kim, A. Celedon, G.D. Longmore, D. Wirtz, A distinctive role for focal adhesion proteins in three-dimensional cell motility, Nat. Cell Biol. 12 (2010) 598–604, https://doi.org/10.1038/ncb2062.
[32] C.M. Waterman-Storer, Microtubule/organelle motility assays, Curr. Protoc. Cell Biol. (2001) 13.1.1–13.1.21, https://doi.org/10.1002/0471143030.cb1301s00 Chapter 13, Unit 13.1.
[33] S. Xiang, G. Xing, W. Xue, C. Lu, J.-M. Lin, Comparison of two different deposition methods of 3-aminopropyltriethoxysilane on glass slides and their application in the ThinPrep cytologic test, Analyst 137 (2012) 1669, https://doi.org/10.1039/c2an15983j.
[34] A. Edelstein, N. Amodaj, K. Hoover, R. Vale, N. Stuurman, Computer control of microscopes using manager, Curr. Protoc. Mol. Biol. (2010) 1–17, https://doi.org/10.1002/0471142727.mb1420s92.
[35] C.A. Schneider, W.S. Rasband, K.W. Eliceiri, NIH Image to ImageJ: 25 years of image analysis, Nat. Methods 9 (2012) 671–675, https://doi.org/10.1038/nmeth.2089.
[36] National Center for Biotechnology Information, (n.d.). https://pubchem.ncbi.nlm.nih.gov/compound/13521.
[37] M.D. Bartlett, A.J. Crosby, Scaling normal adhesion force capacity with a generalized parameter, Langmuir 29 (2013) 11022–11027, https://doi.org/10.1021/la4013526.
[38] M.D. Bartlett, A.J. Crosby, Material transfer controlled by elastomeric layer thickness, Mater. Horizons 1 (2014) 507, https://doi.org/10.1039/C4MH00106K.
[39] E.E. Antoine, P.P. Vlachos, M.N. Rylander, Tunable collagen I hydrogels for engineered physiological tissue micro-environments, PLoS One 10 (2015), https://doi.org/10.1371/journal.pone.0122500.
[40] B.A. Harley, J.H. Leung, E.C.C.M. Silva, L.J. Gibson, Mechanical characterization of collagen-glycosaminoglycan scaffolds, Acta Biomater. 3 (2007) 463–474, https://doi.org/10.1016/j.actbio.2006.12.009.
[41] M.G. Haugh, C.M. Murphy, R.C. McKiernan, C. Altenbuchner, F.J. O'Brien, Crosslinking and Mechanical Properties Significantly Influence Cell Attachment, Proliferation, and Migration Within Collagen Glycosaminoglycan Scaffolds, Tissue Eng. Part A 17 (2011) 1201–1208, https://doi.org/10.1089/ten.tea.2010.0590.
[42] S.P. Carey, C.M. Kraning-Rush, R.M. Williams, C.A. Reinhart-King, Biophysical control of invasive tumor cell behavior by extracellular matrix microarchitecture, Biomaterials 33 (2012) 4157–4165, https://doi.org/10.1016/j.biomaterials.2012.02.029.
[43] A.J. Engler, L. Richert, J.Y. Wong, C. Picart, D.E. Discher, Surface probe measurements of the elasticity of sectioned tissue, thin gels and polyelectrolyte multilayer films: correlations between substrate stiffness and cell adhesion, Surf. Sci. (2004) 142–154, https://doi.org/10.1016/j.susc.2004.06.179.
[44] S. Sen, A.J. Engler, D.E. Discher, Matrix strains induced by cells: computing how far cells can feel, Cell. Mol. Bioeng. 2 (2009) 39–48, https://doi.org/10.1007/s12195-009-0052-z.
[45] J.M. Maloney, E.B. Walton, C.M. Bruce, K.J. Van Vliet, Influence of finite thickness and stiffness on cellular adhesion-induced deformation of compliant substrata, Phys. Rev. E 78 (2008) 041923, https://doi.org/10.1103/PhysRevE.78.041923.
[46] A. Buxboim, K. Rajagopal, A.E.X. Brown, D.E. Discher, How deeply cells feel:

methods for thin gels, J. Phys. Condens. Matter 22 (2010) 194116, https://doi.org/10.1088/0953-8984/22/19/194116.
[47] C.A. Mullen, T.J. Vaughan, K.L. Billiar, L.M. McNamara, The effect of substrate stiffness, thickness, and cross-linking density on osteogenic cell behavior, Biophys. J. 108 (2015) 1604–1612, https://doi.org/10.1016/j.bpj.2015.02.022.
[48] W.S. Leong, C.Y. Tay, H. Yu, A. Li, S.C. Wu, D.H. Duc, C.T. Lim, L.P. Tan, Thickness sensing of hMSCs on collagen gel directs stem cell fate, Biochem. Biophys. Res. Commun. 401 (2010) 287–292, https://doi.org/10.1016/j.bbrc.2010.09.052.
[49] M.S. Rudnicki, H.A. Cirka, M. Aghvami, E.A. Sander, Q. Wen, K.L. Billiar, Nonlinear strain stiffening is not sufficient to explain how far cells can feel on fibrous protein gels, Biophys. J. 105 (2013) 11–20, https://doi.org/10.1016/j.bpj.2013.05.032.
[50] P.H.siu G. Chao, S.C. Sheng, W.R. Chang, Micro-composite substrates for the study of cell-matrix mechanical interactions, J. Mech. Behav. Biomed. Mater. 38 (2014) 232–241, https://doi.org/10.1016/j.jmbbm.2014.01.008.
[51] C.G. Tusan, Y.H. Man, H. Zarkoob, D.A. Johnston, O.G. Andriotis, P.J. Thurner, S. Yang, E.A. Sander, E. Gentleman, B.G. Sengers, N.D. Evans, Collective cell behavior in mechanosensing of substrate thickness, Biophys. J. 114 (2018) 2743–2755, https://doi.org/10.1016/j.bpj.2018.03.037.
[52] M. Miron-Mendoza, J. Seemann, F. Grinnell, The differential regulation of cell motile activity through matrix stiffness and porosity in three dimensional collagen matrices, Biomaterials 31 (2010) 6425–6435, https://doi.org/10.1016/j.biomaterials.2010.04.064.
[53] K.E. Kubow, A.R. Horwitz, S.I. Fraley, Y.F. Feng, D. Wirtz, G.D. Longmore, Reducing background fluorescence reveals adhesions in 3D matrices, Nat. Cell Biol. 13 (2011) 5–7, https://doi.org/10.1038/ncb0111-5.
[54] D. Joaquin, M. Grigola, G. Kwon, C. Blasius, Y. Han, D. Perlitz, J. Jiang, Y. Ziegler, A. Nardulli, K.J. Hsia, Cell migration and organization in three-dimensional in vitro culture driven by stiffness gradient, Biotechnol. Bioeng. 113 (2016) 2496–2506, https://doi.org/10.1002/bit.26010.